ARTICLE IN PRESS
JID:NUPHA AID:21565 /FLA [m1+; v1.298; Prn:8/05/2019; 9:29] P.1 (1-13)
Available online at www.sciencedirect.com
ScienceDirect
Nuclear Physics A ••• (••••) •••–•••
NUCLEAR PHYSICS A
www.elsevier.com/locate/nuclphysa

The ^{48}Ca+^{181}Ta reaction: Cross section studies and investigation of neutron-deficient $86 \leq Z \leq 93$ isotopes

A.K. Mistry [a,b], J. Khuyagbaatar [a,b], F.P. Heßberger [a], D. Ackermann [c], B. Andel [d,1], S. Antalic [d], M. Block [a,b,e], P. Chhetri [a,f], F. Dechery [c], C. Droese [a,g], Ch.E. Düllmann [a,b,e], F. Giacoppo [a,b], J. Hoffmann [a], O. Kaleja [e,h], N. Kurz [a], M. Laatiaoui [b,a], L. Lens [e,a], J. Maurer [a], P. Mosat [d], J. Piot [c], S. Raeder [a,b], M. Vostinar [c], A. Yakushev [a], Z. Zhang [i]

[a] *GSI Helmholtzzentrum für Schwerionenforschung, 64291 Darmstadt, Germany*
[b] *Helmholtz-Institut Mainz, 55099 Mainz, Germany*
[c] *GANIL, 14076 Caen Cedex, France*
[d] *Comenius University in Bratislava, 84248 Bratislava, Slovakia*
[e] *Johannes Gutenberg-Universität, 55099 Mainz, Germany*
[f] *Technische Universität Darmstadt, 64289 Darmstadt, Germany*
[g] *Universität Greifswald, 17489 Greifswald, Germany*
[h] *Max-Planck-Institut für Kernphysik, 69117 Heidelberg, Germany*
[i] *Institute of Modern Physics, Chinese Academy of Sciences, 730000 Lanzhou, China*

Received 8 March 2019; received in revised form 1 May 2019; accepted 2 May 2019

Abstract

Fusion-evaporation reactions with the doubly magic projectile ^{48}Ca were used to access neutron-deficient nuclei around neptunium at the velocity filter SHIP, and investigated using the COMPASS decay spectroscopy station. With the use of digital electronics, several isotopes produced via neutron, proton, and α evaporation channels were identified by establishing correlated α-decay chains with short-lived sub-μs members. Data are given on decay chains stemming from ^{225,226}Np, ^{225}U, and ^{222,223}Pa. New information on the isotopes ^{225,226}Np and ^{222}Pa was obtained. Production cross sections of nuclei in the region using a variety of projectiles are discussed. The measured production cross-sections indicate that the usual advantages of using ^{48}Ca as a beam projectile to produce nuclei $Z > 100$ are absent in the production of these slightly lighter nuclei.

E-mail address: A.K.Mistry@gsi.de (A.K. Mistry).
[1] Present address: KU Leuven, Instituut voor Kern- en Stralingsfysica, B-3001 Leuven, Belgium.

https://doi.org/10.1016/j.nuclphysa.2019.05.003
0375-9474/

Please cite this article in press as: A.K. Mistry et al., The ^{48}Ca+^{181}Ta reaction: Cross section studies and investigation of neutron-deficient $86 \leq Z \leq 93$ isotopes, Nucl. Phys. A (2019), https://doi.org/10.1016/j.nuclphysa.2019.05.003

Keywords: Heavy-ion induced fusion; Alpha decay; Digital electronics for nuclear spectroscopy

1. Introduction

The doubly magic ^{48}Ca (Z=20, N=28) nucleus is an essential ingredient in the experimental synthesis of heavy and superheavy nuclei in fusion-evaporation reactions. Thus its reaction properties are of high interest in the quest to locate the next region of spherical nuclei with enhanced stability above ^{208}Pb, predicted to be around proton numbers $Z = 114$ or 120, and neutron numbers $N = 184$ or 172. Ref. [1] provides a comprehensive discussion on the various theoretical models and their predictions. The uniqueness of ^{48}Ca as a projectile in fusion-evaporation reactions at Coulomb barrier energies is purely due to its underlying nuclear structure and neutron excess. The double magicity and neutron richness allows one to produce the heaviest nuclei with relatively more neutrons than with other projectiles. As a result, many transfermium ($Z > 100$) nuclei have been produced using ^{48}Ca, and the experimentally obtained nuclear and atomic information has aided in improving the underlying model basis for the properties of superheavy nuclei (see [2,3] and refs. therein). Of long-standing interest in the broader scope of nuclear structure physics is the heavy neutron-deficient region of the nuclear chart towards the neutron N=126 shell closure (see Fig. 1). The motivations behind such studies are to evaluate the influence of the shell closure on the underlying nuclear properties with increasing Z. To produce such nuclei can be done either directly using fusion-evaporation reactions, or indirectly via multi-nucleon transfer reactions. The former, in particular, have predominately been used to produce neutron-deficient nuclei in this region albeit with low production cross sections (e.g. [4,5]). Indeed, ^{48}Ca has rarely been used to produce such nuclei (see [6] for an example where it was used to produce ^{226}U 30 years ago), most likely due its neutron richness. However, based on the advantages of ^{48}Ca in the superheavy region, in combination with proper target nuclei, it may still prove to be a reasonably good projectile to produce nuclei in the neutron-deficient heavy N=126 region. The primary limitation of experimental advances in this region was previously due to the short-lived α-emitters in decay chains, which result from relatively high Q_α values. Therefore, in addition to the challenge of low production cross-sections, experimental techniques to register very short-lived events were required to map full decay chains and continue the experimental drive in the exploration of this region. With the advent of data acquisition systems involving fast sampling electronics, sub-μs lifetime measurements are now feasible, with pulse-shape analysis techniques used to extract decay times and energies (see e.g. [4,7,8]). In Fig. 1, the region of interest in our work is shown in the expanded window, and the isotopes produced with their decay chain members are highlighted. Nuclei now accessible thanks to digital electronics (i.e. ns to 20 μs regime) are indicated by the red shading.

Only recently are data available in this region on the production of extremely neutron-deficient nuclei using ^{40}Ar [5,9] and ^{50}Ti [4] projectiles. In a continuation of these studies, ^{48}Ca was used in combination with ^{181}Ta ($Z = 73$, $N = 108$) target material to produce a variety of neutron-deficient nuclei in the vicinity around neptunium (Np, Z=93). We obtained data for full decay chains stemming from ^{225,226}Np (where only tentative information existed [10,11]), and the other populated reaction channels of ^{225}U, and ^{222,223}Pa. Furthermore, an assessment on the applicabil-

Please cite this article in press as: A.K. Mistry et al., The ^{48}Ca+^{181}Ta reaction: Cross section studies and investigation of neutron-deficient 86 ≤ Z ≤ 93 isotopes, Nucl. Phys. A (2019), https://doi.org/10.1016/j.nuclphysa.2019.05.003

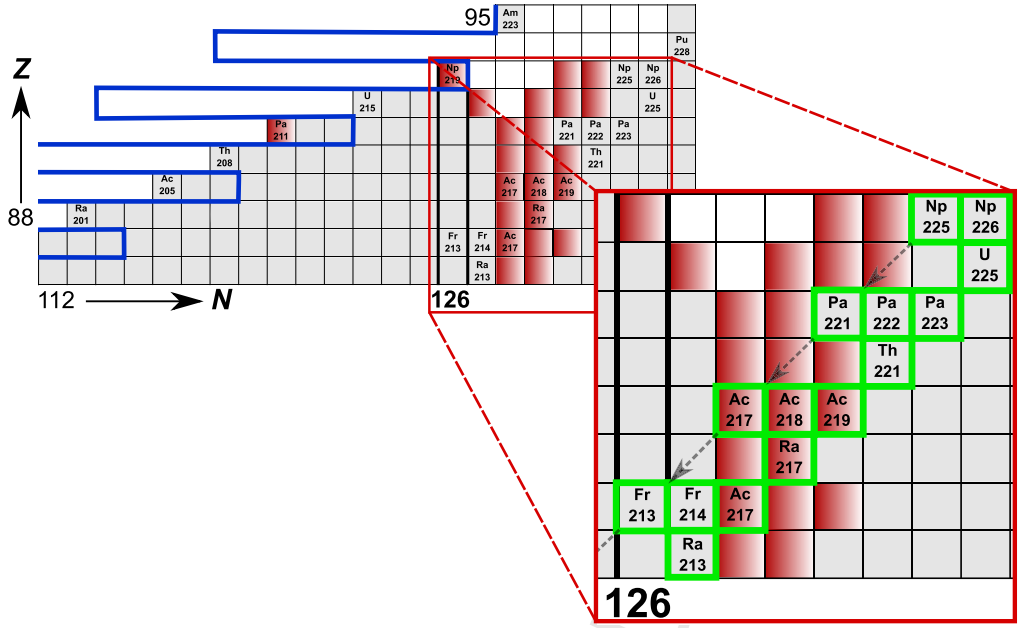

Fig. 1. (*Colour online*) Excerpt from the chart of nuclides showing the isotopes of interest in the neutron-deficient region close to N=126. An indication of the location of the proton dripline is shown by the solid blue lines representing the proton separation energies obtained from [12]. The gradient colour in the squares represents nuclei with half-lives <20 µs. The nuclei measured in this study are given in the expanded pane highlighted by the green boxes. Dashed arrows give an illustrative example for the decay chains stemming from the production of ^{225}Np. White spaces indicate currently unknown nuclei.

ity of ^{48}Ca for producing nuclei in this region with comparisons to the alternative beam projectile candidates of ^{40}Ar and ^{50}Ti, as well as ^{40}Ca and ^{44}Ca is discussed.

2. Experimental setup

The study was performed at the SHIP velocity filter [13] located behind the UNILAC accelerator at GSI Helmholtzzentrum für Schwerionenforschung, Germany. A pulsed ^{48}Ca beam (5 ms wide at a 5 Hz repetition rate) was impinged on ^{181}Ta target material. The target was mounted in segments on a wheel rotating synchronously with the beam macro structure. The target segments consisted of layers of ^{181}Ta with a thickness of ≈530 µg/cm^2, sandwiched between carbon layers with thicknesses of 50 µg/cm^2 upstream and 10 µg/cm^2 downstream backing. Three different beam energies were selected based on cross-section predictions using the HIVAP code [14], such that the centre-of-target energies were 212 MeV (total beam dose 1.97×10^{17} particles), 217 MeV (3.14×10^{16} particles) and 226 MeV (2.67×10^{16} particles). The compound nucleus formed in the reaction was ^{229}Np*. Based on the chosen beam energies, we expected to measure the highest yield of nuclei in xn, αxn and pxn reaction channels corresponding to ^{225}Np (4n evaporation channel), ^{225}U (p3n) and ^{224}Np (5n) respectively. After de-excitation via the evaporation of particles, the evaporation residues (ERs) were separated from the ^{48}Ca primary beam by SHIP and delivered to the focal plane of the separator. An estimated transmission efficiency of the separator ϵ_{SHIP}≈40% was used for the cross-section evaluation of the neutron and/or proton

Please cite this article in press as: A.K. Mistry et al., The ^{48}Ca+^{181}Ta reaction: Cross section studies and investigation of neutron-deficient 86 ≤ Z ≤ 93 isotopes, Nucl. Phys. A (2019), https://doi.org/10.1016/j.nuclphysa.2019.05.003

evaporation channels. In the case of αxn evaporation channels the transmission is expected to be significantly lower due to the recoiling effect of the α particle on the heavy ion [15]. After separation, the ERs travelled through two time-of-flight (ToF) detectors before being implanted into the COMPAct Spectroscopy Set-up (COMPASS) [16]. The apparatus comprises a Double-sided Silicon-Strip Detector (DSSD) as an implantation detector (60×60 strips with a 1 mm^2 pixel size) for the measurement of ER implantations and subsequent α decays. The DSSD was surrounded by 4 Single-sided Silicon-Strip Detectors (SSSDs) upstream to the DSSD in an open cube formation covering 85% of 4π to register the backward emitted α particles from the DSSD. The calibration of the Si detectors was performed using the α decay of implanted ^{254}No residues produced in the ^{48}Ca+^{208}Pb reaction and the subsequent decay products ^{250}Fm and ^{246}Cf. In order to extract events in the case of 'fast' decays ($\leq$ 40 µs), the differential signals from the preamplifiers connected to the detectors were delivered to FEBEX pipelining ADC modules [17] with a 50 MHz sampling rate and a total trace window length of 40 µs. The energy of the signals was extracted using pulse-shape analysis in the form of a trapezoidal filter detailed in Ref. [18], with the minimum detection threshold set at 100 keV. The signal traces were treated by two different filters depending upon the time difference between neighbouring signals. For signals that were $\geq$10 µs apart, a single-signal filter provides a better energy resolution for a single trace while for shorter separated signals, a multi-signal filter was necessary to avoid a pile up of the trapezoidal shape at the consequence of a degraded energy resolution. An example of such filters can be found in [16].

3. Alpha decay data

The following section gives an overview of the measured data and the methods applied for isotope assignments. In previous studies (which applied different data acquisition electronics), an assessment of complete decay chains could not be performed due to the short-lived nature of the chain members. With digital electronics this is now possible. Most of the expected decay chains for this study contain short-lived nuclei (100 ns–10 µs) which will result in at least one event assigned as a pile-up due to the trace size of 40 µs. Accordingly, 'pile-up events' are defined here as two or more signals in a given trace window. We selected conditions within the correlation analysis and performed a detailed trace inspection for each of the events, always requiring at least one pile-up event to be present. Candidates for correlated α-decay chains were searched for with the criteria of an event within the same pixel or one of the neighbouring pixels of the DSSD (in the case of signal charge splitting, measured to be $\sim$10% [16]) in the chosen time window. The search time windows were varied depending on the applied correlation types and are given below. Events with traces containing two or three signals are defined here as pile-up events ($\alpha - \alpha$), and ($\alpha - \alpha - \alpha$) respectively. Once the non-random chains were found, their isotopic assignments were made based on the energies and decay times of the members in comparison with the literature data. The ER signals were required to have an energy range E=10 – 40 MeV in coincidence with the ToF signals. The lifetimes of the respective isotopes were extracted using the universal curve distribution described in [19]. In the following subsections, each chain assignment and their decay properties are discussed. A graphical summary of the chains assigned in this study is given in Fig. 2 (excluding ^{225}Np which is given in Fig. 5) with the literature data given in the yellow boxes for comparison. A summary of all correlation conditions applied is given in Table 1.

Please cite this article in press as: A.K. Mistry et al., The ^{48}Ca+^{181}Ta reaction: Cross section studies and investigation of neutron-deficient $86 \leq Z \leq 93$ isotopes, Nucl. Phys. A (2019), https://doi.org/10.1016/j.nuclphysa.2019.05.003

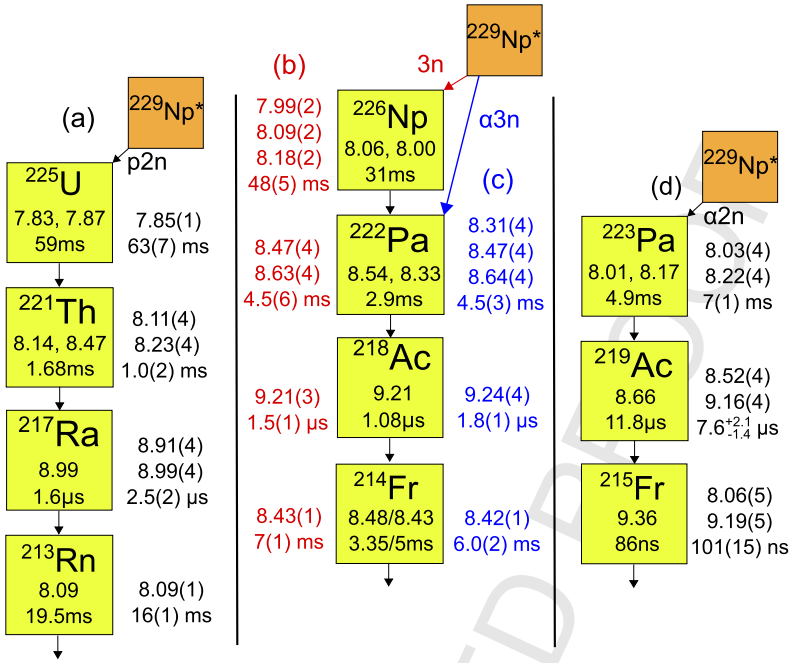

Fig. 2. (*Colour online*) Decay chains measured in this study (^{225}Np chains are shown separately in Fig. 5). Energies are given in MeV. The ^{229}Np* box represents the compound nucleus. The literature energy and half-life values are given inside the boxes, while the values measured in this study are listed outside for (a) and (b) ER$-\alpha_1-(\alpha_2-\alpha_3)-\alpha_4$, (c) ER$-(\alpha_1-\alpha_2)-\alpha_3$ and (d) ER$-(\alpha_1-\alpha_2-\alpha_3)$.

Table 1
A table summarising the applied search criteria for each isotope. The time conditions (T_{con}) are given for the portion of the decay chain they apply to. The energy condition (E_{con}) is given for the specific chain member applied to. See text for more details.

Decay pattern	E_{con} (MeV)	T_{con} (ms)		ER
ER$-(\alpha_1-\alpha_2)-\alpha_3$	7–9 (α_3)	50	Δt(ER$-\alpha_1-\alpha_2-\alpha_3$)	^{222}Pa
ER$-\alpha_1-(\alpha_2-\alpha_3)-\alpha_4$	7–9 (α_4)	500 200	Δt(ER$-\alpha_1$) $\Delta t(\alpha_2-\alpha_3)-\alpha_4$	^{226}Np/^{225}U
ER$-(\alpha_1-\alpha_2-\alpha_3)$	0.1-20 (pile-up)	100	Δt(ER$-(\alpha_1-\alpha_2-\alpha_3)$)	^{223}Pa
ER$-(\alpha_1-\alpha_2-\alpha_3)-\alpha_4$	6-8 (α_4)	100 3.5×10^5	Δt(ER$-(\alpha_1-\alpha_2-\alpha_3)$) $\Delta t(\alpha_1-\alpha_2-\alpha_3)-\alpha_4$	^{225}Np

3.1. Chains stemming from ^{222}Pa

The assignment of chains stemming from ^{222}Pa (Fig. 2(c)) produced in the α3n evaporation channel of the reaction was determined from the α-decay energy and half-life of the final α_3 member of the chain. The decay chain has the pattern ER$-(\alpha_1-\alpha_2)-\alpha_3$, such that the α_1 and α_2 events pile up. In Fig. 3, the energies and time distributions extracted for the events are shown in the left and right panels respectively. In the case of α_3, a well pronounced single peak at 8.42(1) MeV was detected due to the use of the single-signal energy filter, whereas for α_1

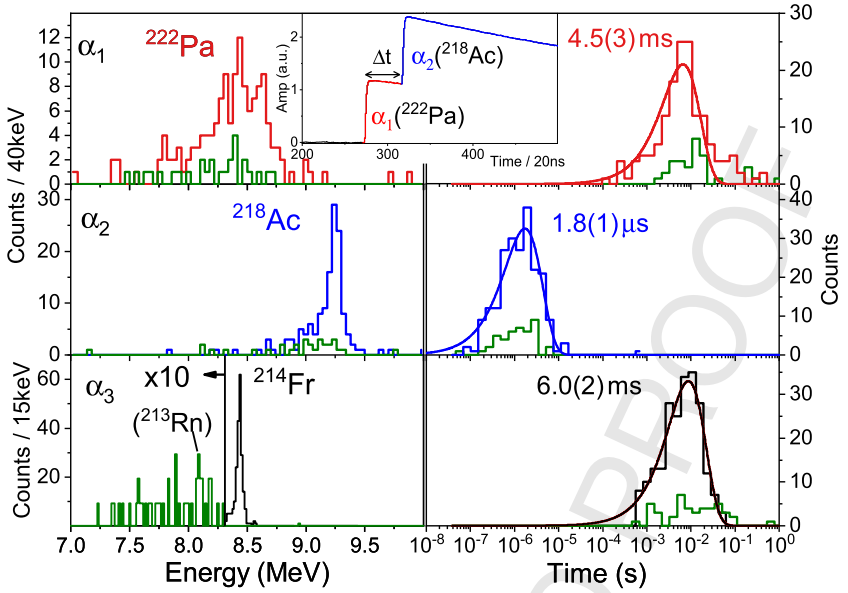

Fig. 3. (*Colour online*) Left panels: Energy distributions correlated to the final α_3 event shown in the bottom left panel for events with the signature ER$-(\alpha_1$-$\alpha_2)-\alpha_3$. In the right panels the timing distributions (Δt) are shown for each chain member with the fitted time distribution and the half-life given. An example pile-up trace is shown in the inset. Based on the energy and time distributions, the assignment to the chain stemming from ^{222}Pa (events given in blue) was made. Blue are events assigned to ^{218}Ac and in green are events correlated with the α_3 decay in the range E_{α_3}=(7.0 – 8.3) MeV and (8.6 – 9.0) MeV.

and α_2 the multi-signal filter was required due to the short timing between events (see inset of Fig. 3 for an example signal trace). Comparing the well-defined α_3 decay energy and half-life with the literature values [20–22], ^{214}Fr was attributed to being the origin of the α_3 decay. Accordingly, the other members were assigned to originate from the α decays of ^{218}Ac(α_2) and ^{222}Pa(α_1). Hence, these chains were attributed to originate from the decay of the directly implanted ^{222}Pa. In general, a relatively wide energy distribution of the α_1 events was observed, while their Δt distributions seemingly show the presence of only one activity. The isotopic assignments for ^{222}Pa and ^{218}Ac are further supported by the literature data given in [23–26], albeit with slightly differing energies and half lives. For ^{222}Pa, the half-life measured falls approximately inbetween the two disagreeing literature values in [23,24], whereas for the ^{218}Ac, a larger value is measured. However, again, the literature values vary somewhat (see Table 2). No events at the corresponding energy for the I^{π}=8$^-$ isomer known in ^{214}Fr were observed (E=8.477, 8.546 MeV $T_{1/2}$=3.35(5) ms [27]). Only the energy and time of events correlated with the α_3 energy range E=(8.3 – 8.6) MeV were used in the ^{222}Pa chain assignment. However some additional events broadly distributed within the energy range of 7.2 – 8.2 MeV for α_3 are evident. In Fig. 3 these latter events are shown in green along with their preceding α_1 and α_2 correlated events. These events could potentially originate from either a decay chain of ^{221}Th based on the similar half-lives and energies of the two chains, or from the decay chain of ^{225}U, if α_1 escapes and is unrecorded. Nevertheless a definitive assignment cannot be made due to the rather broad energy spread of the α_3 events.

Please cite this article in press as: A.K. Mistry et al., The ^{48}Ca+^{181}Ta reaction: Cross section studies and investigation of neutron-deficient 86 ≤ Z ≤ 93 isotopes, Nucl. Phys. A (2019), https://doi.org/10.1016/j.nuclphysa.2019.05.003

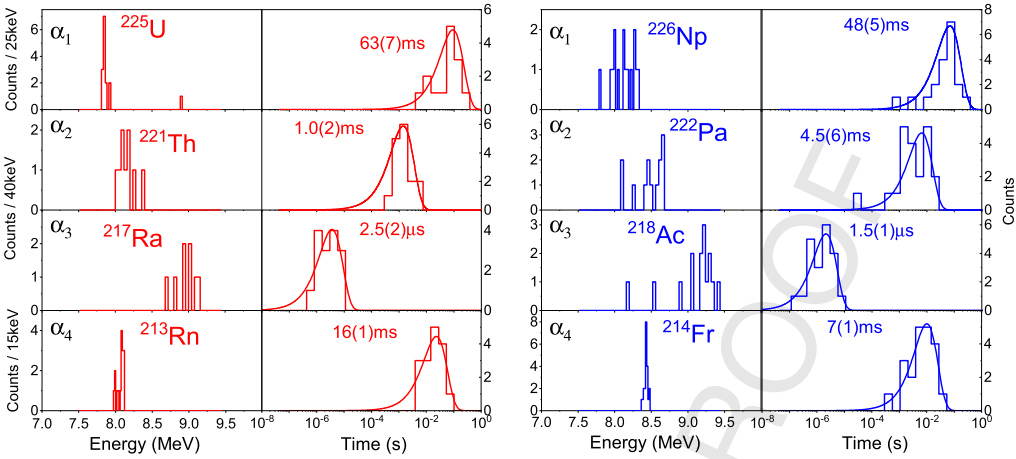

Fig. 4. (*Colour online*) Energy and time spectra of the chains with the decay signature ER$-\alpha_1-(\alpha_2$-$\alpha_3)-\alpha_4$ with chains stemming from ^{225}U given in red and ^{226}Np in blue, respectively. The members of the decay chains were identified based on correlations to the α_4 events (^{213}Rn and ^{214}Fr) shown in the bottom panels.

3.2. *Chains stemming from ^{226}Np and ^{225}U*

Decay chains of the signature ER$-\alpha_1-(\alpha_2-\alpha_3)-\alpha_4$ were observed such that a preceding α-decay and a final α_4 decay occurred in delayed coincidence with the $(\alpha_2-\alpha_3)$ pile-up signal. The isotopic identification of these chains was obtained in a similar way described in section 3.1, while here the decay properties of the α_4 chain members were used.

For the applied correlation conditions, we observed two well separated peaks at energies 8.09(1) MeV and 8.43(1) MeV with half-lives 16(1) ms and 7(1) ms, respectively, for the α_4 decays (see Fig. 4 bottom panels). We identified these peaks as being the α decays of ^{213}Rn and ^{214}Fr after comparison with literature data given in [28–30] and [20–22] respectively. Consequently, the corresponding members of the chains leading down to ^{213}Rn and ^{214}Fr (α_4) were assigned to the decay of ^{217}Ra and ^{218}Ac (α_3), ^{221}Th and ^{222}Pa (α_2), stemming from implantations of ^{225}U and ^{226}Np (α_1), produced by the p3n and 3n evaporation channels respectively. One can note that despite strongly overlapping decay characteristics (energy and half-life distribution) of ^{217}Ra and ^{218}Ac, and ^{221}Th and ^{222}Pa, it was possible to isolate the individual decays (*cf*. Fig. 4) due to the separated energies of the events (α_4) terminating the decay chains. The single-signal filter was used to obtain the α_1 decay energies and a well pronounced peak for ^{225}U is evident (Fig. 4 upper left panel) while the energies of α particles associated with the decay of ^{226}Np are relatively broadly distributed. For ^{226}Np, the α_1 events (Fig. 4 top right energy panel) show a broad energy distribution E=(7.9 – 8.4) MeV, however with the signature for three different α-decay transitions with comparable intensities at 7.98(2), 8.09(2) and 8.18(2) MeV. This could correspond to either single α decay activities or to α-decay+conversion electron summing. The half-life for ^{226}Np was determined to be 48(5) ms. This is not in agreement with [32] 31(8) ms. Such a complex α-decaying fine structure can be attributed to the odd-N and odd-Z nature of the nucleus (as can also be seen for the ^{222}Pa α-decay lines in Fig. 3 upper left panel). One α-decaying transition group for ^{226}Np was found in [32] at $\sim$ 8.044(20) MeV, however two transitions are given in [31] at E=8.00 MeV and 8.06 MeV, however no decay time is given, and

Please cite this article in press as: A.K. Mistry et al., The ^{48}Ca+^{181}Ta reaction: Cross section studies and investigation of neutron-deficient 86 $\leq Z \leq$ 93 isotopes, Nucl. Phys. A (2019), https://doi.org/10.1016/j.nuclphysa.2019.05.003

no information on the experimental conditions or methodology is presented for the measured nuclei in the given citation.

The ^{222}Pa daughter of ^{226}Np was also produced directly (see in the previous subsection) in the α3n evaporation channel. In a comparison of ^{222}Pa α-decay events in Fig. 3 and ^{222}Pa in Fig. 4, one can note a relatively well enhanced peak-like structure for ^{222}Pa at around 8.5 MeV and 8.6 MeV following production via ^{226}Np, which is different than the very broadly distributed energies from the direct production. Thus one can suggest that the ^{222}Pa state decaying by an 8.31 MeV α transition, populated during direct production, is potentially not populated (or weakly populated) by the decay of ^{226}Np. To draw firm conclusions, enhanced data are required.

In the present study, 16 α-decay events with energy E=7.85(1) MeV were attributed to the ground-state to ground-state transition of ^{225}U into ^{221}Th, and are shown in Fig. 4 upper left panel. The half-life 63(7) ms measured in our study is in agreement with the values given in [28] (59^{+5}_{-2} ms) but not with that in [22] (84(4) ms). In the literature data, both sources are in agreement with three α-decay transitions found at 7.621, 7.833 and 7.868 (15) MeV [28]. The 7.621 MeV transition was relatively weak in the given studies (5(2)%), however we did not confirm the second transition with energy E=7.833 MeV (37(5)%) given in [28,22]. A possible reason for this is that this transition is attributed to decay into a $9/2^+$ excited level in ^{221}Th, which then decays into the $7/2^+$ ground-state via an M1 electromagnetic transition, which proceeds primarily via conversion electron emission. Since a ^{22}Ne projectile was used in both [28,22], the ERs were implanted closer to the detector surface and thus the influence of α-decay energy summing with conversion electrons was lower compared to our study. We note that 3 events were found for ^{213}Rn at an energy of $\sim$ 7.98(1) MeV whereas in the literature data only one primary transition has been observed at $\sim$ 8.090 MeV [28,29,22].

3.3. Chains stemming from ^{225}Np

More convoluted pile-up events were detected, whereby three α particles could be detected in the same trace window. In total 29 signals were found to have three events in a pile up, with two of the signals then having additional α_4 decays 45 s and 13 s after the pile-up event. The energies of the α_4 events were E=6.75(1) MeV and 6.73(1) MeV, which after comparison with literature data was likely to be ^{213}Fr (6.775 MeV [22], $T_{1/2}$ = 34.14(6) s [33]). Based on this, and the subsequent extraction of the energies and times from the triple pile-up trace, we assign these two chains to stem from ^{225}Np. The remainder of the 27 chains is assigned to stem from ^{223}Pa.

^{225}Np was first reported in 1992 [10] having an α-decay energy of 8.63(2) MeV. However, no information was given on the half-life or correlation conditions used for the assignment. More recently, ^{225}Np was produced in the decay chains of ^{233}Bk and ^{229}Am via a multi-nucleon transfer reaction [11]. In this case, a half-life of $3.3(^{+7.6}_{-2.7})$ ms was determined, but without energy information based on two events due to the fast decaying members of the chains. While both studies [10] and [11] have claimed to have identified the isotope, both energy and half-life were not simultaneously determined. In the present experiment, we assigned both energy and half-life simultaneously across both chains which are illustrated together with the trace details in Fig. 5. The half-life of $T_{1/2}$=$0.31(^{+0.75}_{-0.13})$ ms extracted from the mean lifetime of the two cases is somewhat shorter, but still consistent with that given in [11]. The α-decay energy of E=8.8(1) MeV extracted from one event can be attributed to ^{225}Np. For ^{221}Pa, in chain (a) there was an undetected α-particle escape from the detector with only partial energy deposition while in chain (b) the α-decay energy differs significantly from the literature value given in [34,35]. In the given

Please cite this article in press as: A.K. Mistry et al., The ^{48}Ca+^{181}Ta reaction: Cross section studies and investigation of neutron-deficient 86 $\leq Z \leq$ 93 isotopes, Nucl. Phys. A (2019), https://doi.org/10.1016/j.nuclphysa.2019.05.003

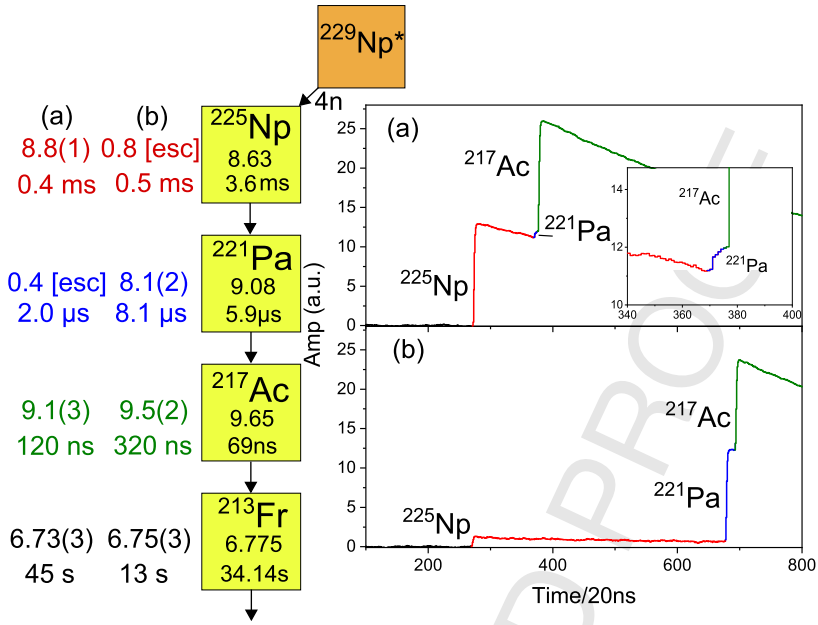

Fig. 5. *(Colour online)* The decay chain assigned to ^{225}Np observed in this study. The extracted energies and half-lives for traces (a) and (b) are given on the left, and the literature values are given in the yellow squares. For chain (a) an examination of the pile-up trace shows that the ^{225}Np and ^{217}Ac α-decay signals were recorded as full events, but the ^{221}Pa α particle in this case escapes. With chain (b), an α_1 escape is followed by the full α-decay energy signals assigned to ^{221}Pa and ^{217}Ac. No events in the box detectors were recorded. The two chains were assigned based on the final ^{213}Fr decay within the same pixel. Energies are given in MeV.

reference data for ^{221}Pa, the sum of ^{221}Pa+^{217}Ac ($\sim$ 18.8 MeV) energies was taken (separately unresolvable due to the pile up) and subsequently the energy of ^{217}Ac was used to determine the ^{221}Pa decay energy. Thus one ought to be cautious on the precision from such a method in terms of the influence of calibration effects. To confirm the validity of the chain assignment, an assessment of the background was done and the probability of the chains being random was determined to be 5×10^{-4}. Furthermore there were no other decay chain patterns found in the region that could have similar decay properties to this one.

The additional 27 pile-up chains with three signals were assigned to stem from the ER implantation of ^{223}Pa with the decay signature ER$-(\alpha_1 - \alpha_2 - \alpha_3)$. Two peaks corresponding to ^{223}Pa α decays were resolved at E=8.03(4) MeV and 8.22(4) MeV, respectively with the half-life of 7(1) ms extracted from all events. This is supported by the literature data with energies 8.014(5) MeV and 8.172(5) MeV [36] and the half-life of 6.5(10) ms given in [24]. All measured data are summarised in Table 2.

4. Production cross-sections

The nuclei identified in this work are produced in different evaporation channels of the compound nucleus (CN) ^{229}Np* formed in the ^{48}Ca+^{181}Ta fusion reaction. By using the number of identified chains, the beam integrals, the efficiencies for the detection of full energy α particles in the DSSD and/or DSSD+SSSDs and the transmission efficiency of SHIP (details given in

Please cite this article in press as: A.K. Mistry et al., The ^{48}Ca+^{181}Ta reaction: Cross section studies and investigation of neutron-deficient 86 $\leq Z \leq$ 93 isotopes, Nucl. Phys. A (2019), https://doi.org/10.1016/j.nuclphysa.2019.05.003

Table 2
Summary of the decay data obtained in this study. The literature information can be found in the given references. Literature values are given in square brackets for the cases where data deviates from this study. [a), b)] and [c)] indicate the relevant reference.

Isotope	E (keV)	$T_{1/2}$	Ref
^{226}Np	7.99(2), 8.09(2), 8.18(2)	48(5) [[a)]31(8)] ms	[a)][32][31]
^{225}Np	8.8(1)	$0.31^{+0.75}_{-0.13}$ ms	[10][11]
^{225}U	7.85(1) [[a),b)]7.621, 7.833, 7.868(15)]	63(7) [[b)]84(4) ms]	[a)][28] [b)][30]
^{223}Pa	8.03(4), 8.22(4)	7(1) [[a)]4.9(4)] ms	[24] [a)][36]
^{222}Pa	8.47(4), 8.63(4) [[a)]8.16-8.21, 8.54, 8.33(15) [b)]8.18]	4.5(3) ms [[a)]5.7(5), [b)]$2.9(^{+0.6}_{-0.4})$] ms	[a)][24] [b)][23]
^{221}Pa	8.1(2) [9.08(3)]	$3.5^{+8.5}_{-1.4}$ µs	[34][35]
^{221}Th	8.11(4), 8.23(4)	1.0(2) ms [[b)]1.68(6), [b)]$2.0^{+0.3}_{-0.2}$, [c)]1.73(3)] ms	[a)][27] [b)][30] [c)][28]
^{219}Ac	8.52(4), 9.16(4)	$7.6^{+2.1}_{-1.4}$ µs	[24][34]
^{218}Ac	9.22(3)	1.8(1) µs [[a)]0.27(4), [b)]1.21(18), [c)]1.31(12)] µs	[a)][24][b)][25][c)][26]
^{217}Ac	9.3(2)	150^{+370}_{-60} ns	[37][38]
^{217}Ra	8.91(4), 8.99(4)	2.5(2) [[a)]1.6(2)] µs	[27] [a)][29]
^{215}Fr	8.06(5), 9.19(5) [[a)]9.355(10), [b)]9.369(10)]	101(15) [[a)]120(2)] ns	[a)][39] [b)][40]
^{214}Fr	8.43(1)	6.0(2) ms	[20][21][22]
^{213}Fr	6.74(2)	20^{+48}_{-8} s	[22]
^{213}Rn	7.98(1), 8.09(1)	16(1) [[a)]25(2)] ms	[28] [a)][29][30]

section 2), the production cross-sections of ^{225,226}Np isotopes corresponding to the 3n and 4n reaction channels respectively, were obtained.

The evaluated cross-sections of the 3n and 4n evaporation channels of ^{40}Ar, ^{40,44,48}Ca, and ^{50}Ti induced reactions with nuclear deformed ^{151}Eu–^{182,184,186}W targets are shown in Fig. 6. Only the maximum cross-sections of either the 3n or 4n channels were considered to minimise the effects of the collision orientation of the target, and the coupling of the low-lying states in the reactants in the fusion process. Data from literature are shown by the squares, while present data (^{48}Ca+^{181}Ta) are shown by triangles. In addition, as a part of the same study, a ^{nat}W ($Z = 74$, $N = 182, 184, 186$) target was also utilised to measure chains of nuclei around neutron-deficient plutonium Pu (decay chains are detailed in [41]), which is also included, given with triangles. The majority of the known data follows an exponentially decreasing cross-section trend of production with increasing Z of the CN as shown by the dashed fitted trend lines in the same figure for CN $Z \leq 90$. However, when one takes into account CN $Z > 90$ for these targets, it can be seen

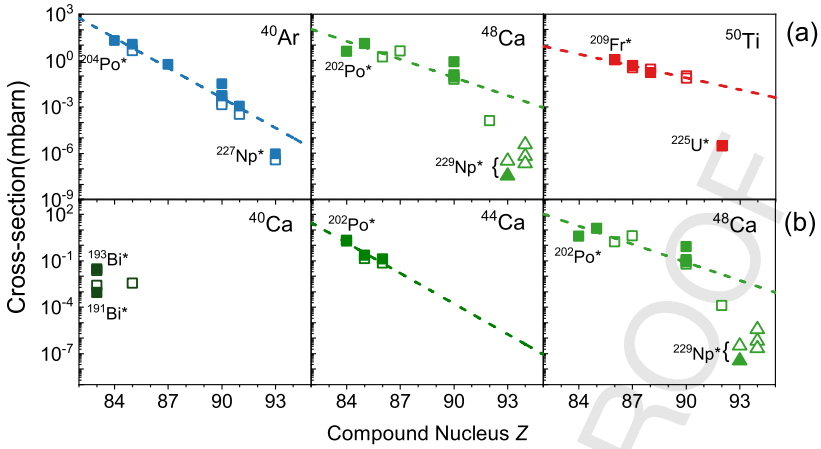

Fig. 6. (*Colour online*) Comparison of production cross section maxima in the 3n (open symbols) and 4n (filled symbols) evaporation channels from CN Z=83–94. a) ^{40}Ar, ^{48}Ca and ^{50}Ti projectile induced reactions [42–46,4]. b) ^{40,44,48}Ca (^{44,48}Ca data from [47]). The experimental values from this study (including measurements from [41]) are given by the triangles. The dashed straight lines show fits for data CN $Z \leq$90.

that the cross-section values break away from the trend, which ultimately decreases with heavier projectiles, particularly for ^{48}Ca and ^{50}Ti. From the data in this study, the newly measured cross-section data for the production of neutron-deficient Np isotopes (and the Pu data from [41]) do not follow the expected trend but lie significantly lower. This deviation could be associated with the reduced survival probability of the compound nuclei as suggested in [48], where it is discussed that a decrease in the fission barrier is responsible. The newly added data from this study for the ^{48}Ca projectiles supports this hypothesis. Considering the cross sections with lighter Ca isotopes in Fig. 6b), it can be seen that cross sections are further reduced as one moves away from the N=28 neutron shell closure for Ca. However the lack of data in this region is also evident, and more data is required before drawing any explicit conclusions. Taking into the account the comparison among projectiles that could potentially be used to synthesize neutron-deficient nuclei in this region, it can be concluded that ^{40}Ar is a more favourable selection, despite the enhanced shell stabilisation effects associated with Ca (and in particular ^{48}Ca).

5. Conclusion

We have studied fusion-evaporation reactions with the ^{48}Ca projectile to produce neutron-deficient actinide nuclei. ^{225,226}Np, ^{225}U, and ^{222,223}Pa, which were produced in the xn, pxn and αxn channels, respectively, were identified and their decay properties measured by applying modern fast digital electronics. The decay chains were identified using trace analysis techniques. The data discussed is generally confirmed by literature values while new information is given on ^{226,225}Np and the α-decaying structure of ^{222}Pa as well as new data on some half-lives. Exploration of nuclei along the N=126 shell closure is hindered not only due to short half-lives, but also due to low production rates. This was highlighted by a comparison of nuclei produced with various beam projectiles via the fusion-evaporation mechanism for this region of the nuclear chart, emphasizing the sharp drop in the production cross sections, in part due to a decrease in survival probability of the compound nucleus. Despite the low cross-sections that deviate from the typical exponential decrease, ^{40}Ar can be considered more favourable for producing neutron-

Please cite this article in press as: A.K. Mistry et al., The ^{48}Ca+^{181}Ta reaction: Cross section studies and investigation of neutron-deficient 86 $\leq Z \leq$ 93 isotopes, Nucl. Phys. A (2019), https://doi.org/10.1016/j.nuclphysa.2019.05.003

deficient nuclei in the heavy region above the N=126 shell closure, and experimental efforts will continue in this fashion. Of interest for further studies would be to perform systematic studies with other, more neutron (and proton) deficient projectiles to do a full assessment of the impact on the production of nuclei in this region.

Acknowledgements

We thank the UNILAC staff as well as the ion source crew for delivering beams of high and stable intensity. We are also grateful to J. Steiner, B. Lommel, and A. Hübner for production of the large area targets. We want to express our gratitude to H.G. Burkhard and J. Maurer for skilful maintenance of the mechanical and electrical components of SHIP. Three of us, SA, BA and PM, were supported by the Slovak Research and Development Agency (Contract No. APVV-14-0524) and the Slovak Grant Agency VEGA (Contract No. 1/0532/17). Three of us (MV, JP, FD) were supported by the French-German Collaboration agreement IN2 P3 - DSM/CEA and GSI No. 15-73. One of us, D.A., is supported by the European Commission in the framework of the CEA-EUROTALENTS Program 2014-2018 (noPCOFUND – GA – 2013 - 600382).

References

[1] P.-H. Heenen, et al., Nucl. Phys. A 944 (2015) 415–441.
[2] M. Asai, F.P. Heßberger, A. Lopez-Martens, Nucl. Phys. A 944 (2015) 308–332.
[3] Yu.Ts. Oganessian, V.K. Utyonkov, Nucl. Phys. A 944 (2015) 62–98.
[4] J. Khuyagbaatar, et al., Phys. Rev. Lett. 115 (2015) 242502.
[5] M.D. Sun, et al., Phys. Lett. B 771 (2017) 303.
[6] F.P. Heßberger, et al., Z. Phys. A 333 (1989) 111.
[7] A. Såmark-Roth, et al., Phys. Rev. C 98 (2018) 044307.
[8] H.B. Yang, et al., Eur. Phys. J. A 55 (2019) 8.
[9] T.H. Huang Physet, et al., Phys. Rev. C 98 (2018) 044302.
[10] A.N. Andreyev, et al., AIP Conf. Proc. 250 (1992) 499.
[11] H.M. Devaraja, et al., Phys. Lett. B 748 (2015) 199.
[12] P. Möller, et al., At. Data Nucl. Data Tables 125 (2019) 1–192.
[13] G. Münzenberg, et al., Nucl. Instrum. Methods 161 (1) (1979) 65.
[14] W. Reisdorf, M. Schädel, Z. Phys. A Hadrons Nucl. 343 (1992) 47.
[15] W. Faust, et al., Nucl. Instrum. Methods 166 (3) (1979) 397.
[16] D. Ackermann, et al., Nucl. Instrum. Methods A 907 (2018) 81.
[17] J. Hoffmann, et al., GSI Sci. Rep. 253 (13) (2011).
[18] V. Jordanov, G.F. Knoll, Nucl. Instrum. Methods A 345 (2) (1994) 337.
[19] K.-H. Schmidt, Eur. Phys. J. A 8 (2000) 141.
[20] D.F. Torgerson, R.A. Gough, Phys. Rev. 174 (4) (1968).
[21] K. Valli, E.K. Hyde, Phys. Rev. 176 (4) (1968).
[22] P. Kuusiniemi, et al., Eur. Phys. J. A 23 (2005) 417.
[23] K.-H. Schmidt, Nucl. Phys. A 318 (1979) 253.
[24] J. Borggreen, et al., Phys. Rev. C 2 (1970) 1841.
[25] N. Schultz, et al., Phys. Rev. C 28 (1983) 1.
[26] M.E. Debray, et al., Phys. Rev. 39 (1989) 1193.
[27] D.F. Torgerson, R.D. Macfarlane, Nucl. Phys. A 149 (3) (1970) 641.
[28] F.P. Heßberger, et al., Eur. Phys. J. A 8 (4) (2000) 521.
[29] K. Valli, E.K. Hyde, J. Borggreen, Phys. Rev. C 1 (1970) 6.
[30] P. Kuusiniemi, et al., Acta Phys. Pol. B 32 (2001) 1009.
[31] A.N. Andreyev, et al. (Eds.), Proc. 6th Intern. Conf. on Nuclei Far from Stability, vol. 759, 1993.
[32] V. Ninov, et al., Z. Phys. A At. Nucl. 336 (4) (1990) 473.
[33] M. Fisichella, et al., Phys. Rev. C 88 (2013) 011303(R).
[34] H. Miyatake, et al., Nucl. Phys. A 501 (3) (1989) 557.

Please cite this article in press as: A.K. Mistry et al., The ^{48}Ca+^{181}Ta reaction: Cross section studies and investigation of neutron-deficient $86 \leq Z \leq 93$ isotopes, Nucl. Phys. A (2019), https://doi.org/10.1016/j.nuclphysa.2019.05.003

[35] R. Hingmann, et al., Z. Phys. A At. Nucl. 313 (1) (1983) 141.
[36] F. Hoellinger, et al., Phys. Rev. C 60 (5) (1999) 057301.
[37] T. Nomura, et al., Nucl. Phys. A 217 (1973) 253.
[38] D.J. Decman, et al., Nucl. Phys. A 436 (1985) 311.
[39] T. Nomura, et al., Phys. Rev. C 9 (1974) 1168.
[40] D.J. Decman, et al., Nucl. Phys. A 419 (1984) 163.
[41] A.K. Mistry, et al., Acta Phys. Pol. B 49 (2018) 613.
[42] C.C. Sahm, et al., Nucl. Phys. A 442 (2) (1985) 316.
[43] D.A. Mayorov, et al., Phys. Rev. C 90 (2014) 24602.
[44] H.W. Gäggeler, et al., Nucl. Phys. A 502c (1989) 561.
[45] Yu.Ts. Oganessian, et al., Phys. Rev. C 90 (2013) 034605.
[46] D.A. Mayorov, et al., Phys. Rev. C 92 (2015) 054601.
[47] A.V. Yeremin, et al., Nucl. Instrum. Methods A 350 (1994) 608.
[48] J. Khuyagbaatar, EPJ Web Conf. 163 (2017) 00030.

Please cite this article in press as: A.K. Mistry et al., The ^{48}Ca+^{181}Ta reaction: Cross section studies and investigation of neutron-deficient $86 \leq Z \leq 93$ isotopes, Nucl. Phys. A (2019), https://doi.org/10.1016/j.nuclphysa.2019.05.003